Determination of the internalization pathway of photoluminescent nanodiamonds in mammalian cells for biological labeling and optimization of the fluorescent yield.

Orestis Faklaris, Vandana Joshi, Theano Irinopoulou, Patrick Tauc, Hugues Girard, Celine Gesset, Mohamed Senour, Alain Thorel, Jean-Charles Arnault, Jean-Paul Boudou, et al.

Determination of the internalization pathway of photoluminescent nanodiamonds in mammalian cells for biological labeling and optimization of the fluorescent yield

Orestis Faklaris [⋆], *Vandana Joshi* [†], *Theano Irinopoulou* [¶], *Patrick Tauc* [§], *Hugues Girard* [‡], *Celine Gesset* [‡], *Mohamed Senour* [♭], *Alain Thorel* [♭], *Jean-Charles Arnault* [‡], *Jean-Paul Boudou*[†], *Patrick A. Curmi* [† *], *and François Treussart* [⋆ *]

[⋆] O. Faklaris, Prof. F. Treussart
Laboratoire de Photonique Quantique et Moléculaire, UMR CNRS 8537, Cachan (France)

[†] Dr. V. Joshi, Dr. J.-P. Boudou, Dr. P.A. Curmi
Laboratoire Structure et Activité des Biomolécules Normales et Pathologiques, Université Evry-Val-d'Essonne and INSERM U829, Evry (France)

[¶] Dr. T. Irinopoulou
Institut du Fer à Moulin, UPMC Univ. Paris 6 et INSERM, UMR-S 839 (France)

[§] Dr. Patrick Tauc
Laboratoire de Biologie et de Pharmacologie Appliquée,
Ecole Normale Supérieure de Cachan, CNRS UMR 8113, Cachan, (France)

[‡]Dr. H. Girard, Dr. C. Gesset, Dr. J.C. Arnault
Diamond Sensor Laboratory,
Centre d'Etudes Atomiques, Gif-sur-Yvette, France

[♭]Dr. M. Sennour, Dr. A. Thorel,
Laboratoire Pierre-Marie Fourt CNRS UMR 7633,
Centre des Matériaux de l'Ecole des Mines de Paris, Evry (France)

[*] corresponding authors: P.A. Curmi and F. Treussart
pcurmi@univ-evry.fr
francois.treussart@ens-cachan.fr

Abstract

Diamond nanoparticles have been recently used as new fluorescent labels in cells. Their emission relies on color centers embedded in the diamond matrix. In this work we compare the photoluminescence of a single color center embedded in a 30 nm diameter nanodiamond to that to a single dye molecule and demonstrate the perfect photostability of the color centers. We also compare the photoluminescence properties of nanodiamonds prepared under different conditions in order to find the optimal parameters to achieve a high fluorescence yield. We use these photoluminescent nanodiamonds for HeLa cell labeling and investigate their uptake mechanism. On the one hand by immunostaining the endocytotic vesicles and on the other by transmission electron microscopy observations we study the localization of nanodiamonds in cells. Moreover, by blocking selectively different endocytotic mechanisms we unravel their internalization pathway. We find that nanodiamonds enter the cells by receptor-mediated endocytosis. The results of this study are a prerequisite for the use of photoluminescent nanodiamonds as intracellular markers or drug delivery devices.

Key words: diamond nanoparticles, photoluminescence, biolabel, endocytosis, confocal microscopy

Introduction

Nanoparticles hold great promises for future biomedical applications, notably due to the possibility to combine biological and inorganic materials with the prospect to develop innovative diagnostic tools and therapies. Among them, nanoparticles like quantum dots (1, 2, 3), gold nanobeads (4, 5), silicon beads (6) can be used to label with high specificity biomolecules, to track their fate in cell culture systems and organisms or even to deliver bioactive molecules or drugs that may otherwise remain not deliverable.

In this context, the development of new nanoparticles to label biomolecules at the single molecule scale would represent a significant step for efficient *in vivo* long term tracking of biomolecules. Apart from radioisotopes which present obvious drawbacks such as toxicity, particular care in handling and disposal, organic dyes and fluorophores are widely used to label biomolecules, but they photobleach rapidly under continuous illumination (7), which makes difficult quantification and long term follow-up. Semiconductor nanocrystals, or Quantum Dots (QDs), have a better stability and a lower photobleaching yield. They also offer the possibility of multicolor staining by size tuning (8). However such nanoparticles may be cytotoxic at long term scale due to their chemical composition (9) and present the important drawback of photoluminescence intermittency (photoblinking) which again makes difficult the efficient tracking of individual nanoparticles (10).

In contrast photoluminescent nanodiamonds (PNDs) are promising alternative biomarkers. Their photoluminescence results from embedded nitrogen-vacancy color centers (NV) in the diamond matrix (11) which present a perfect photostability with no photobleaching or photoblinking. Their remarkable photoluminescence properties allow reliable single particle tracking in live cells (12, 13, 14), as it has been demonstrated that such PNDs easily penetrate cells in culture. The low cytotoxicity of nanodiamonds produced by High Pressure and High Temperature (HPHT) (15, 16) and of nanodiamonds produced by detonation (17, 18) has also been demonstrated.

Moreover, thanks to their long fluorescence decay lifetime (15-25 ns), time gated imaging is possible, which can improve significantly the signal to noise ratio for intracellular imaging (16).

Together, the remarkable photoluminescence properties of PDNs combined with the possibility to perform various chemical treatments to modify their surfaces to graft bioactive moieties (19, 20, 21) and with the possibility to produce them massively with tiny sizes (22) give to PNDs the potential for multiple applications to biology, for example as markers of different intra or extra cellular compartments or as long term traceable delivery vehicles for biomolecules translocation in cell (18, 20, 21).

Despite the outstanding perspectives opened by PNDs in various fields of biology, including drug delivery and therapeutic applications, it seems to us that a better knowledge and control of the process that renders diamond nanoparticles photoluminescent together with an understanding of the mechanism underlying the cellular uptake is still missing, despite its crucial importance for future use of PNDs in drug delivery and therapeutic applications.

The present work addresses both issues and is thus divided in two parts. Firstly a detailed qualitative and quantitative comparison of the photoluminescent properties of single dye molecules and single NV centers in nanodiamonds is carried out, demonstrating the photostability of the NV center and extracting useful conclusions on its photoluminescence yield.

To further improve the NV photoluminescence yield, we change the irradiation parameters and increase the NV concentration per nanodiamond.

In the second part, we carry out the first systematic investigation of the cellular uptake and pathway of PNDs in model cell lines (HeLa cells). With special cells treatment we block endocytosis and then

with the use of specific drugs we inhibit the receptor mediated endocytotic procedures. The results show that the internalization of PNDs stems mainly on receptor-mediated endocytosis, which may be enhanced in our case by the adsorption of serum proteins on the nanodiamonds surface.

We finally report a high level of colocalization of PNDs with endosomes and lysosomes in particular for the biggest particles. A small portion however of the smallest nanoparticles is found to be localized outside these vesicular systems.

Materials and Methods

Production of Photoluminescent Nanodiamonds and surface functionalization

The PNDs used in this work were of two types (listed in table 1). For type 1 the starting material was synthetic type Ib diamond powder (SYP 0-0.05, Van Moppes, Geneva) with a specified size smaller than 50 nm. NDs are made photoluminescent following the procedure described in Ref. (23). Briefly, the creation and stabilization of NV centers were performed by high energy proton irradiation (irradiation doses 5×10^{15} H^+/cm^2 and 5×10^{16} H^+/cm^2) and subsequent annealing at 800°C under vacuum ($\sim 10^{-8}$ Torr) for 2 hours. Deagglomeration of PNDs was then achieved by strong acid treatment (H_2SO_4:HNO_3, 1:1 vol:vol, at 75°C for 3 days) followed by pure water rinsing steps. By centrifugation process we selected the smaller PNDs. We observed in this fraction an average size below 50 nm, as determined by Atomic Force Microscopy (*Nanoscope IIIa*, Veeco Instruments Inc., USA) and Transmission Electron Microscopy (TEM device is a Tecnai F20-ST microscope operating at 200 kV) (Fig. 1). This acid treatment also allows us to obtain a stable suspension of NDs in deionized water, probably related to repulsive electrostatic interactions between charged surface chemical groups, mainly carboxylic groups (15). The ζ-potential in aqueous solution was -41.3 mV (measured with a Zetasizer Nano ZS from Malvern) and the hydrodynamic radius 30 nm (measured with the DL135 particle size analyzer by Dynamic Light Scattering, Cordouan Technologies). The size calculation with DLS measurements yielded the hydrodynamic radius of the particles, considering them spherical, which is not always the case as it is seen on the TEM images.

For type 2 PNDs the starting material was type Ib diamond highly crystalline synthetic micron size powder (Element Six) with a specified size of 150-200 μm. NV centers were created in the microcrystals by high energy electron irradiation (2×10^{19} e^-/cm^2) and subsequent annealing under vacuum (800°C, 2 h). Diamond microcrystals were then reduced in size by nitrogen jet milling to obtain submicron crystals (Hosokawa-Alpine, Germany). Further size reduction to nanoparticles was achieved by ball milling under argon, using a planetary ball mill (Fritsch, Germany, for more details on the procedure look Ref. (22)). The milled powder was then sieved and treated by strong sonication at 50°C, followed by a HNO_3 attack for one day at 75°C. After a series of rinsing cycles with pure water, filtration and multiple centrifugations, we achieved to have PNDs with average size of 46 nm (DLS measurement). AFM imaging showed many type 2 single PNDs with smaller dimensions (10-15 nm) but the majority appeared aggregated in clusters of 2-3 particles corresponding to an overall size of 40-50 nm, as also seen on TEM images Fig. 1b. These PNDs were stable in deionized water solutions and displayed a ζ-potential equal to -43 mV, compatible with the presence of surface carboxylic groups.

Size distribution of PDNs: a) and c) Atomic Force Microscope scan of type 1 and type 2 PNDs respectively; b) and d) High Resolution Transmission Electron Microscope Image of type 1 and type 2 PNDs respectively..

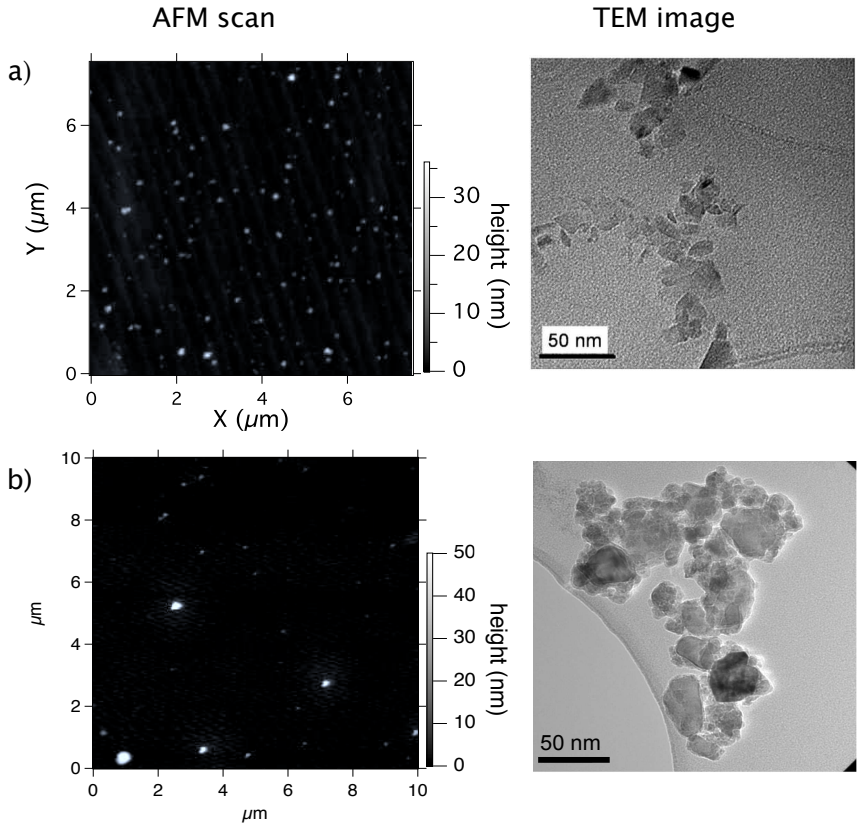

Figure 1: Size distribution of PDNs: a) AFM scan and TEM image of type 1 PNDs; b) AFM scan and TEM image of type 2 PNDs.

PND type	size (nm)	shape	irradiation method	dose	ζ-potential (mV)
1	30	sharp	H^+	5×10^{15} H^+/cm^2 5×10^{16} H^+/cm^2	-41.3
2	46	round	e^-	2×10^{19} e^-/cm^2	-43

Table 1: Types of PNDs used

Comparison of fluorescence properties of organic molecules and PNDs

We evaluate the relative photoluminescence yield of single NV center compared to carbocyanine $DilC_{18}$ (Spectrum Info, CAS No 41085-99-8) and Nile Red 20 nm beads (Molecular Probes). These specific dyes were chosen because their excitation spectrum is close to that of the NV color centers. Samples were prepared by spin coating on glass coverslips of a solution of polymethyl methacrylate (PMMA - 1% mass in anisole) containing dye molecules or a solution of polyvinyl alcohol (PVA - 1% mass) containing diamond nanocrystals. Using this procedure, we obtained a few tens of nanometer thick polymer coating where molecules or PNDs were well separated from each other and could be individually probed.

Photoluminescence of dye molecules and PNDs was probed using a home-built scanning stage confocal microscope. It relies on a Nikon TE300 microscope, converted to a confocal setup with the right modifications. Excitation was achieved either with a continuous-wave (cw) laser, emitting at wavelength of 488 nm or with another cw laser emitting at 532 nm, depending on the application. The objective used was a $\times 60$ Nikon oil immersion microscope objective, 1.4 numerical aperture. Photoluminescence was collected from the sample by the same objective and was spectrally filtered by a long wave pass filter (RazorEdge LP03-488RU-25 or LP03-532RU-25, 97% transmission between 494-1100 or 539-1200 nm for 488 and 532 nm wavelength excitation respectively) and spatially filtered by a 50 μm diameter pinhole. It was then acquired by an avalanche photodiode in the single photon counting mode (SPCM-AQR14; Perkin-Elmer). The number of NV color centers per nanoparticle was measured using photon antibunching experiments, relying on a Hanbury Brown and Twiss time intensity correlator (24). The excitation laser beam was circularly polarized to be insensitive to the different single-emitter dipole orientations, which could have led to some artifact.

Cell culture preparation

HeLa cells were grown in standard conditions on glass coverslips in Dulbecco Modied Eagles Medium (DMEM) supplemented with 10% fetal calf serum (FCS) and 1% penicillin/streptomycin. To study the cellular uptake of PNDs, cells were seeded at a density of 2×10^5 cells/1.3 cm^2 and grown at 37°C in a humidified incubator under 5% CO_2 atmosphere. 24 h after seeding, the PNDs aqueous suspensions were added to the cell culture medium. The cells were grown under similar conditions for an additional period of time (2 h for fluorescence examination and up to 24 h for the cytotoxicity tests). After incubation, the excess of PNDs was removed by washing the cells with phosphate buffer saline (PBS). The cells were then fixed with 4% paraformaldehyde in PBS and mounted on microscope slides for phase contrast and confocal examination.

Cellular uptake of PNDs

For the endocytosis mechanism investigation of PNDs, cells were treated as following:

Low temperature incubation at 4° C: incubation of PNDs with cells was carried out as described above with the solution kept at 4°C instead of 37°C.
Incubation of cells with PNDs under ATP depletion: for the ATP depletion studies the cells were preincubated in PBS buffer solution and supplemented with 10 mM NaN_3 for 30 min at 37°C and then PNDs were added.
Hypertonic incubation: for the hypertonic treatment the cells were preincubated for 30 min in PBS buffer solution and supplemented with 0.45 M sucrose followed by exposure to PNDs at 37°C.
Filipin treatment: the cells were pretreated in PBS buffer solution and supplemented with filipin (5 μg/ml) for 30 min before exposure to PNDs at 37°C.

For immunofluorescence analyses and the localization of PNDs in cells, endosomes were stained with Fluorescein-conjugated Mouse Anti-human Early Endosome Antigen (EEA1) (BD Transduction Laboratories, USA) (25) and lysosomes with LysoTracker Green DND-26 dye (Invitrogen L7526). In the latter case, when cells reached the desired confluence, the medium was replaced with prewarmed medium containing the LysoTracker probe (at 75 nM concentration, following manufacturers procedure). After one hour incubation, the LysoTracker solution was replaced with fresh medium and cells were fixed as described above.

Intracellular fluorescence observations

For intracellular localization and visualization of PNDs, two microscope types were used. The first one was a Leica SPC2 (Manheim, Germany) confocal laser scanning microscope, with a $\times 63$, 1.4 numerical aperture oil immersion objective. We always used 1 Airy Unit for the pinhole diameter. The second microscope was the home-built confocal setup described previously. The latter setup was used to visualize with high sensitivity the single NV centers of PNDs internalized in cells, thanks to the avalanche photodiode used in the single photon counting mode (in contrast to the Leica microscope where the detector is a photomultiplier). The excitation wavelength used in all cases was 488 nm.

The transmission electron microscopy measurements

For the electron microscopy measurements we used a High Resolution -Transmission Electron Microscope (Tecnai F20 operating at 200 keV). Cells were seeded for 24h in standard conditions (the same as for fluorescence experiments). Type 2 PNDs were added in cell solutions and were incubated for 2 hours at 37°C. Cells were then fixed using a solution of paraformaldehyde, glutaraldehyde and phosphate buffer for 45 min at room temperature. After dehydration with a graded series of ethanol, the cells were embedded in EPON resin. Ultrathin sections were cut for a thickness of 100 nm and were stained with 2% uranyl acetate.

Surface characterization of FNDs in serum supplemented media

Acid-treated PNDs (1 mg) were incubated with DMEM containing 10% fœtal calf serum (FCS) and sonicated for 15 min. After two hours of incubation at room temperature and vortexing, PNDs were washed by three successive centrifugations and re-dispersed in pure water. The ζ-potential was measured with a Zetasizer (Nano ZS from Malvern, England). The nanodiamonds-proteins sample was mixed with KBr powder and pressed into pellets which were then placed in an IR cell. The FTIR spectra of the plate were recorded with a FTIR spectrometer (Thermo Nicolet 8700) under a continuous flow of nitrogen to avoid water adsorption on the sample.

The Cytotoxicity test

To evaluate the putative cell toxicity of PNDs, cells were plated at a concentration of 2×10^5 cells/1.3 cm^2 for 24 hours and then treated with various concentrations of type 1 or type 2 PNDs for 24h in 10% serum supplemented medium. We conducted the MTT assay (3-[4,5 -thylthiazol- 2-yl]-2,5-diphenyl-tetrazolium bromide) relying on mitochondrial activity measurement to assess cellular viability (26). A purple color developed within the cells after 2h of incubation with MTT indicates the cleavage of the tetrazolium salt (MTT) by mitochondrial reductance in live cells. The purple formazan crystals are then dissolved in acidified isopropanol and the absorbance of the solution is measured with a Spectrophotometer (Uvikon XL, Specoman) at 570 nm. The absorbance of cells exposed to PNDs was compared to control cells, not exposed to PNDs, which is associated to 100% absorbance. As a positive control we used Lipofectamine (Invitrogen, USA), a substance widely used for cell transfections, but considered as toxic for long exposition times and doses.

Results

Photoluminescence study and characterization of single PNDs

Organic dye molecules are routinely used to label biomolecules (27, 28). Photoluminescent nanodiamonds appear nowadays as promising markers in this field. We thus compared the photoluminescence properties of a single 30 nm nanodiamond containing a single NV center with that of single dye molecule of carbocyanine $DilC_{18}$ (29). Cyanine dyes are often used in biology as biomolecules labels for a variety of applications such as DNA sequencing or to study single molecule dynamics (30, 31, 32).

This specific dye was chosen because its photoluminescence emission peak is centered on 600 nm, close to the NV color center emission spectrum maximum. We also compared fluorescent properties of single NV centers to that of Nile Red doped beads with a size of 20 nm (emission maximum 575 nm)

Fig. 2a shows a confocal raster scan of dye molecules deposited on a glass coverslip. Many isolated spots are observed, most of them corresponding to single molecule emitters. In order to compare the dyes to PNDs photoluminescence, we measured the signal dependence on the excitation power. This task is not trivial, because most dyes photobleach rapidly under exposure to the laser beam at a few μW excitation power. In addition detection efficiency varies and depends on the environment and the molecule dipole orientation, parameters that we cannot control. Fig. 2b displays the counting rate versus excitation intensity for 4 molecules and for $\sim$ 10 kW/cm^2 excitation intensity (20 μW exc. power) before photobleaching.

The sudden diminution of the fluorescence intensity to the background level after some seconds of continuous excitation is the result of photobleaching and confirms the singularity of the examined dye molecule (Fig. 2d).

For a slow intersystem crossing rate, the three-level model gives a fluorescence emission rate R:

$$R(I_{\mathrm{pump}}) = \eta_Q \times \eta_{\mathrm{det}} \frac{k_{21}}{(k_{21}/k_{12}) + (k_{23}/k_{31}) + 1} \quad (1)$$

where η_Q is the quantum yield of the molecule, η_{det} is the overall detection efficiency, and k the corresponding transition rates for the ground (1), excited (2) and triplet state (3) (33, 34). The rate

k_{21} is calculated by the relation $k_{21} = \sigma I_{\text{pump}}/h\nu_{\text{pump}}$, where σ the absorption cross section of the molecule ($\sigma \approx 4 \times 10^{-16}$ cm^2 for cyanine (35)). Taking into account a dependency of k_{31} on I_{pump} of the form $k_{31} = k_{31}(1 + \beta I_{\text{pump}})$ associated to the pumping of higher-energy triplet states from the lower triplet state, our data are well fitted, with $\beta = 2 \times 10^{-4}$ W/cm^2 and $\eta_Q \times \eta_{\text{det}} = 0.10$.

To study a different system than single organic molecules, we examined a sample with Nile Red doped 20 nm beads. The beads were deposited on the glass substrate by spin coating and observed with the home-built confocal setup. Fig. 2e shows the time laps of the fluorescence intensity of one fluorescent bead under cw 40 μW excitation. We clearly see that the fluorescence signal of the beads is much stronger than that of a single DiC_{18} molecule. However, after 20 seconds of illumination the detected signal almost vanishes due to photobleaching. The diminution of fluorescence occurs by steps, indicating the gradual photobleaching of the Nile Red dye molecules embedded in the bead. It should be mentioned that Fig. 2b represents the total counting rate ($R = R_1 + R_2$) versus excitation intensity, while on the other graphs there is only the counting rate R_1 of the first avalanche photodiode.

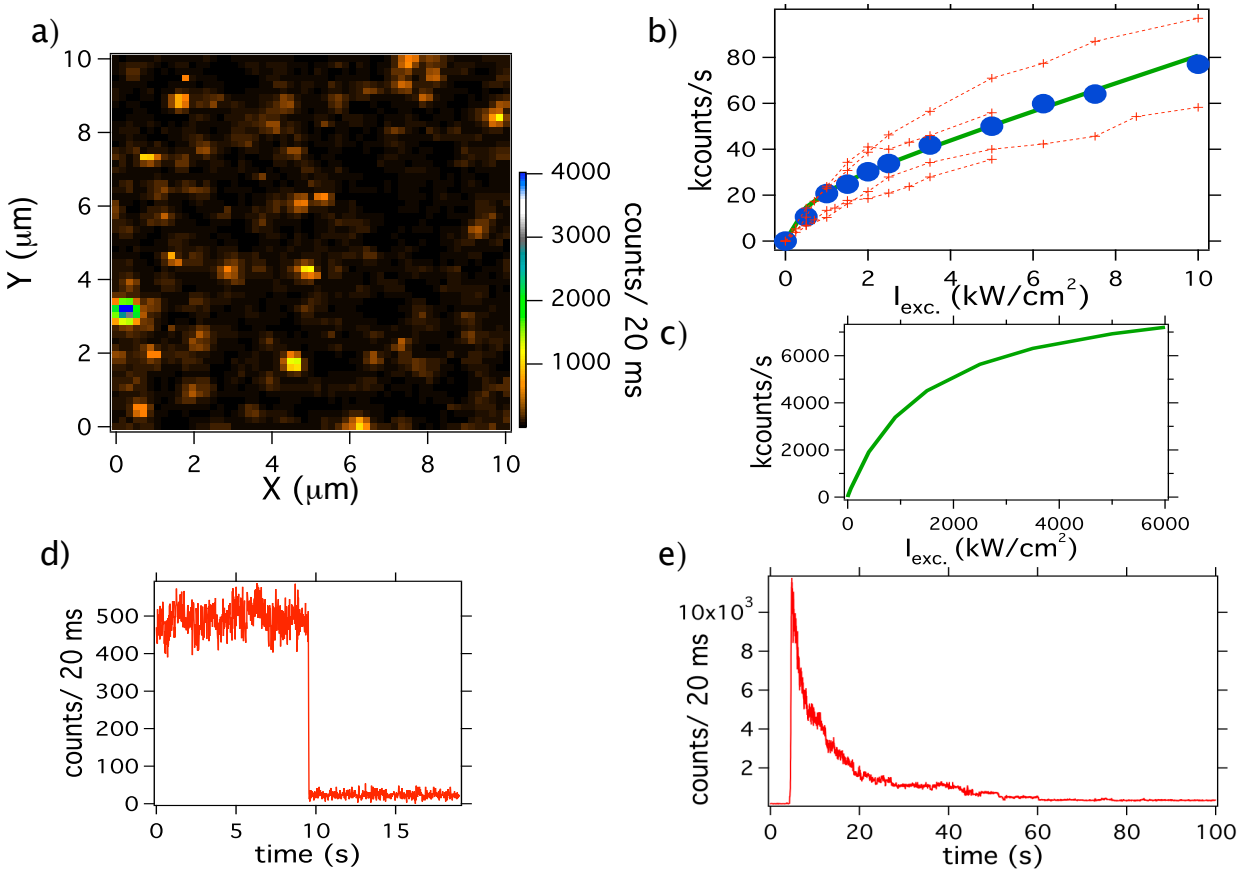

Figure 2: Photoluminescence intensity of single dye molecules deposited on a glass coverslip showing photobleaching: a) Confocal raster scan, cw laser excitation at wavelength 532 nm, excitation power 10 μW (exc. intensity 500 W/cm^2) ; b) Counting rate versus excitation intensity for 4 molecules (dashed colored), with plain green the fit curve according to the three-level model expression; c) Fluorescence saturation curve resulted from the fit (equation(1)) of the mean curve (in green) of b); d) A 20 s emission time trajectory of a single molecule (binning 20 ms) with the characteristic one-step bleaching, cw excitation laser at wavelength 532 nm, exc. power 10 μW; e) Time trace for a 20 nm Nile Red bead, exc. power 40 μW.

We then examined, using the same home-built confocal setup, type 1 PNDs (proton irradiated,

30 nm size distribution). Fig. 3a shows a confocal raster scan of these PNDs, where we observe many photoluminescence spots with different intensities, probably due to an inhomogeneous number of NV centers per nanocrystal. The numbers that appear on the scan next to some spots (on their left) indicate the number of NV centers in the corresponding PNDs, inferred for each nanoparticle from antibunching measurements (24, 36).

Antibunching measurements allowed us to select nanocrystals containing a single NV center (Fig. 3b) and to record its photoluminescence intensity saturation curve. Saturation occurs for excitation power values higher than 3-4 mW (1500-2000 kW/ cm^2) and gives a maximal photoluminescence intensity signal of 55 kcounts/s. As emission rates depend on the environment of the NV center and the NV dipole orientation, we recorded the saturation curve for 3 single NV centers (marked with arrows on the scan) and then calculated the mean value (blue plain). The photoluminescence spectra of the studied PNDs correspond either to the emission of NV^- (Fig. 3c) or NV° color center, identified thanks to their Zero Phonon Line (ZPL) at 637 nm and 575 nm respectively. In both cases, the maximum of the NV emission spectrum lies in the near infrared region (650-700 nm), which is well adapted for biological applications, since in this spectral window cell components and tissues present low absorption.

In contrary to single $DilC_{18}$ molecules or Nile Red beads, we observed that the photoluminescence intensity of a single NV center is perfectly constant over time (Fig. 3e). In the case of a PND containing 4 NV centers we find a 4-5 fold increase of the photoluminescence intensity, which is three times higher than the one of the single cyanine molecule before photobleaching occurs.

Improving the photoluminescence yield of diamond nanocrystals

Active NV centers are created in nitrogen-rich type Ib diamond crystal by a two steps procedure involving the generation of vacancies by electron or ion beams followed by thermal annealing of vacancy defects at temperature $> 600°C$. At such temperatures the vacancies start migrating to the nearest substitutional nitrogen atoms, where their aggregation is energetically favorable (37, 38). The conversion efficiency can however be limited due to competitive processes such as the formation of other defects and vacancy - interstitial recombination.

We attempted here to obtain brighter nanocrystals by varying the irradiation dose of H^+ ions applied to type 1 PNDs. Type Ib nanodiamonds, rich in nitrogen content (∼100 ppm) were irradiated at doses of either 5×10^{15} H^+/cm^2 or 5×10^{16} H^+/cm^2 and then annealed at 800°C for 2 hours. After a size selection by centrifugations we achieved an average PNDs size of 30 nm for both solutions. PNDs were deposited by spin coating on glass coverslips for photoluminescence measurements with the confocal home-built microscope. Fig. 4 shows a comparison of distributions of PNDs emitted intensities for the two irradiation doses. The statistical sampling was 75 and 100 nanoparticles respectively. We found a broad distribution in each case. For the low irradiation dose the median value was 315 kcount/s while it was equal to 986 kcounts/s for an one order of magnitude higher dose, indicating a 3 fold increase of the corresponding photoluminescence signal.

Additionally we calculated the number of NV centers created for each irradiation dose, over a statistical sample of 31 and 48 PNDs respectively. For the low irradiation dose we found a mean value of 2.7±1.1 NV/ nanodiamond and for the high dose the value was 7.0 ± 2.1 NV/ nanodiamond.

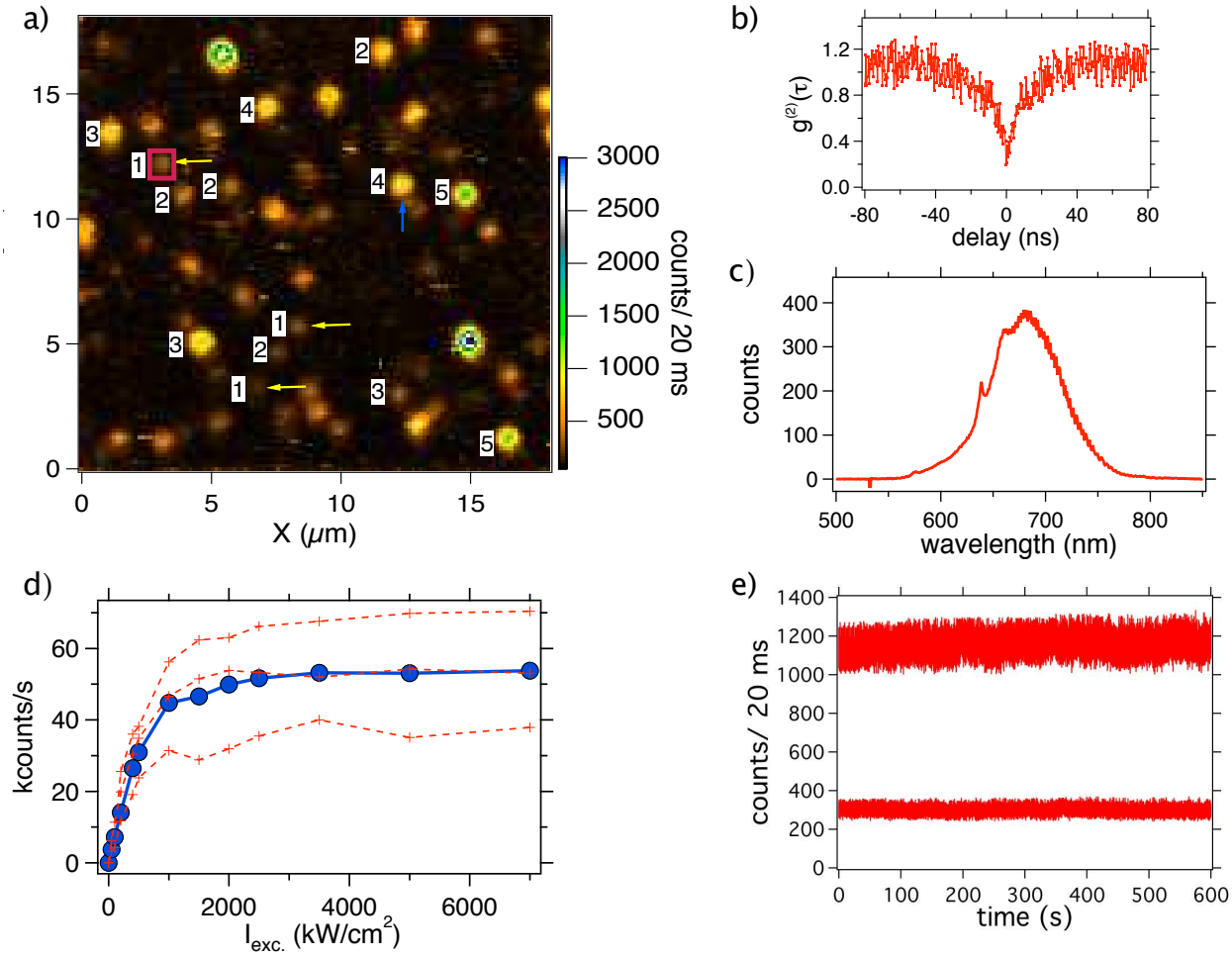

Figure 3: Photoluminescence of a single type 1 PND: a) Confocal raster scan, cw excitation laser at wavelength 532 nm, power 1 mW; the well isolated spots correspond to PNDs; the numbers on the left of the spots correspond to the number of NV centers in each particle; b) Intensity time correlation function of the PND in red square, showing photon antibunching at zero delay associated to the emission of single photons, proving that the studied color center is single; c) Photoluminescence spectrum of the same PND, corresponding to the emission of NV^- color center, identified thanks to its Zero Phonon Line (ZPL) at 637 nm ; d) Saturation curve (plainblue) inferred from the average of 3 single NV center saturation curves (dashed colored); e) Photoluminescence signal of a single NV center and a nanodiamond containing 4 NV centers (marked with vertical blue arrow) over a time period of 600 s, showing the perfect photostability (binning 20 ms).

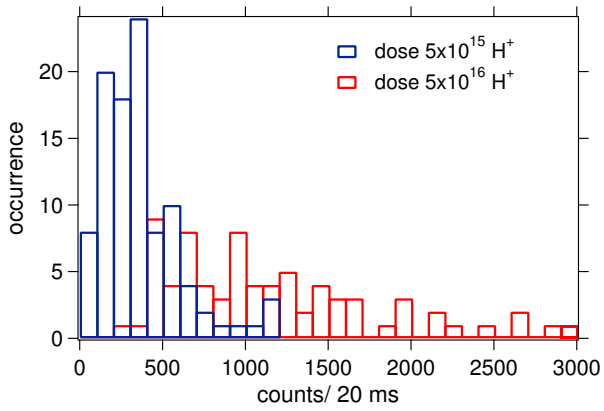

Figure 4: Photoluminescence intensity of smaller than 30 nm PNDs after H^+ irradiation and annealing : a) Occurrence versus photoluminescence intensity for nanodiamonds irradiated with a dose of 5×10^{15} H^+/cm^2; b) Occurrence versus photoluminescence intensity for nanodiamonds irradiated with 5×10^{16} H^+/cm^2.

Investigation of the uptake mechanism of PNDs in HeLa cells

In this work we investigated the internalization mechanism of PNDs in HeLa cells. PNDs can be internalized spontaneously by cells (15, 16, 20). It is known that various extracellular materials enter the cell by endocytosis, an energy-dependent uptake mechanism (39, 40, 41). The mechanism of endocytosis is blocked at low temperature exposure or in ATP (adenosine triphosphate) depleted environment (41, 42).

HeLa cells were thus incubated with PNDs at 37°C, at 4°C or after pretreatment with NaN_3, which disturbs the production of ATP, to evaluate the contribution of endocytosis. We found, using a standard Leica SPC2 confocal microscope, that when endocytosis was hindered by low temperature or NaN_3, the number of PNDs observed in cells decreased dramatically (Fig. 5b,c). Similar results were obtained using the confocal microscope equipped with single photon detectors, which strongly suggest that no or very few PNDs are internalized when endocytosis is blocked. The PNDs used were of type 2, at a concentration of 20 μg/ml. We checked that low temperature exposure of cells actually blocks endocytosis by performing control experiments with transferrin-fluorescein (FITC) conjugates. Transferrin is an 80 kDa serum glycoprotein that mediates iron uptake in vertebrate cells via receptor-mediated endocytosis (43), and labeled transferrin is commonly used to monitor the endocytotic pathway. The results confirmed that in our conditions, transferrin uptake was efficiently blocked at 4°C.

Endocytosis includes various subpathways, like pinocytosis, phagocytosis and receptor mediated endocytosis (RME) (44). In RME a ligand binds onto a cell surface receptor and is internalized as the membrane invaginates. The receptor transports the ligand into the cell, releases it and normally is recycled back to the cell membrane. RME includes clathrin-dependent and clathrin-independent pathways. For clathrin-dependent endocytosis, the clathrin coat on the cell membrane forms invaginations and leads to the budding of clathrin-coated vesicles (44, 45). Clathrin-independent endocytosis occurs mainly through the caveolae pathway (invaginations rich in choresterol (46)).

To enlighten the pathways of the PNDs internalization, cells were incubated with PNDs under conditions that inhibit either the clathrin or the caveolae pathways. Interestingly, we found that pretreatment of cells with sucrose, a hypertonic treatment known to disrupt the formation of clathrin-coated vesicles (47, 48), reduced to a high degree PNDs uptake (Fig. 6a,b).

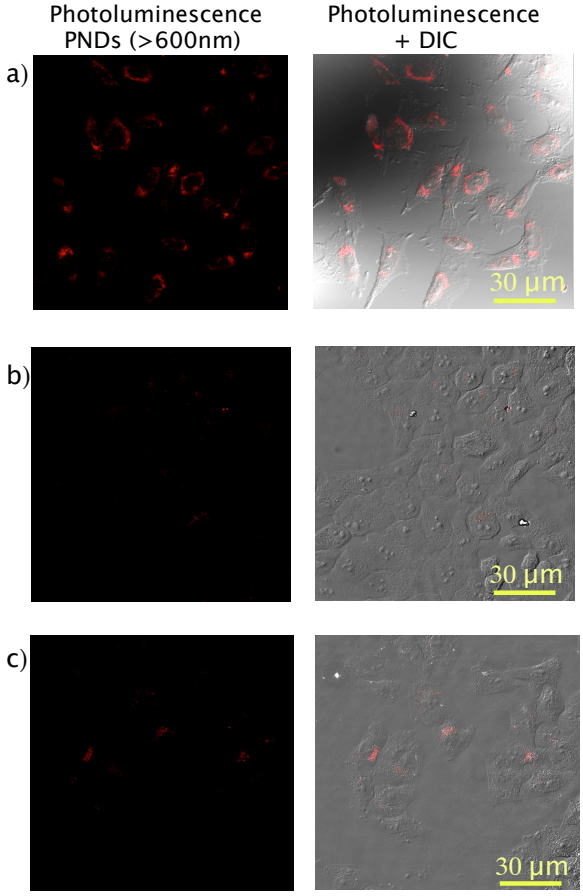

Figure 5: Investigation of PNDs uptake in HeLa cells: a) Confocal raster scan of PNDs incubated with cells at 37°C for 2 hours ; b) Confocal raster scan of PNDs incubated with cells at 4°C for 2 hours ; c) Confocal raster scan of PNDs incubated with cells at 37°C for 2 hours, cells were pretreated with NaN_3; confocal images are acquired at z=1.5 μm above the substrate level, excitation power 0.5 mW, excitation wavelength 488 nm.

To block the caveolae or lipid-rafts pathway, cells were pretreated with filipin. Caveolae-dependent uptake depends on the presence of cholesterol domains. Treatment of cells with filipin disrupts the formation of these domains within the cell membrane. In contrast to the clathrin-blocking experiment, we found that pretreatment with drugs like filipin does not hinder the internalization of PNDs (Fig. 6c,d), suggesting that PNDs are mainly uptaken by the clathrin-mediated pathway.

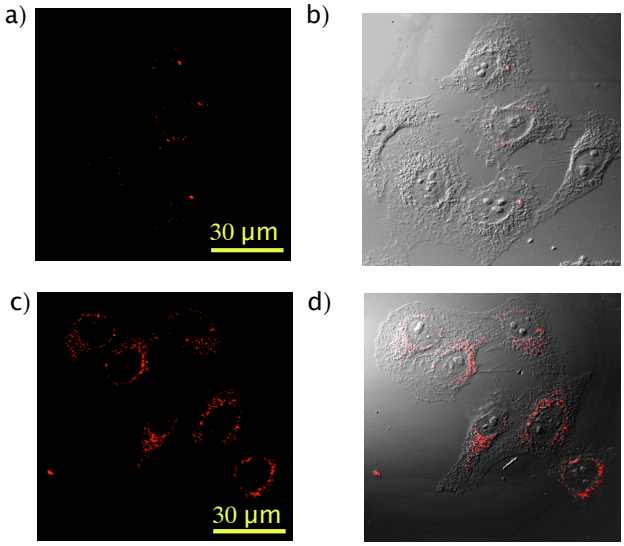

Figure 6: Investigation of PNDs uptake in HeLa cells: a), b) Confocal raster scans of PNDs incubated with cells pretreated with sucrose and c),d) filipin respectively; incubation time 2 hours, at 37°C, excitation power 0.5 mW, excitation wavelength 488 nm.

Intracellular localization of PNDs

Low temperature and NaN_3 experiments strongly suggest that PNDs uptake is a result of an endocytosis mechanism. To better localize cellular compartments associated with PNDs in cells, we performed endosomal and lysosomal immunostaining in PND loaded cells to search for a potential colocalization. Endosomes are the vesicles responsible for the transport of extracellular materials in the cell cytoplasm with the mechanism of endocytosis. After internalization, endosomes are either recycled towards the membrane and the material is free in the cytoplasm or are fused to lysosomes (44). In a previous study we indeed found that type 1 PNDs are partially colocalized with early endosomes (16).

We check in this work these results for type 2 PNDs, which are of different sizes and shapes.

Endosomes were stained with FITC and we collected light in the spectral range 500-530 nm (excitation wavelength 488 nm) while for PNDs we detected signal between 600-750 nm (incubation time with cells: 2 hours). The PNDs concentration was 10 μg/ml. The confocal raster scans acquired with the Leica confocal microscope show a high degree of colocalization of PNDs with the early endosome antigen (Fig. 7a). We performed control experiments and no artificial overlap was observed.

To further elucidate the fate of the smaller and less bright PNDs, we examined the samples with the home-built confocal setup. We found only a partial colocalization implying that some PNDs have never entered or have escaped from the endosomes.

The next step of the endocytotic pathway is the intracellular “digestion” in the lysosomes. Lysosomes were labeled with LysoTracker Green DND-26 dye. After 3 hours incubation of PNDs with

cells, we observed a high degree of colocalization (Fig. 7b). Examination of cells with the confocal setup equipped with avalanche photodiodes showed a partial colocalization of PNDs with lysosomes suggesting that some of them have escaped the endocytosis pathway and may reside in the cell cytoplasm.

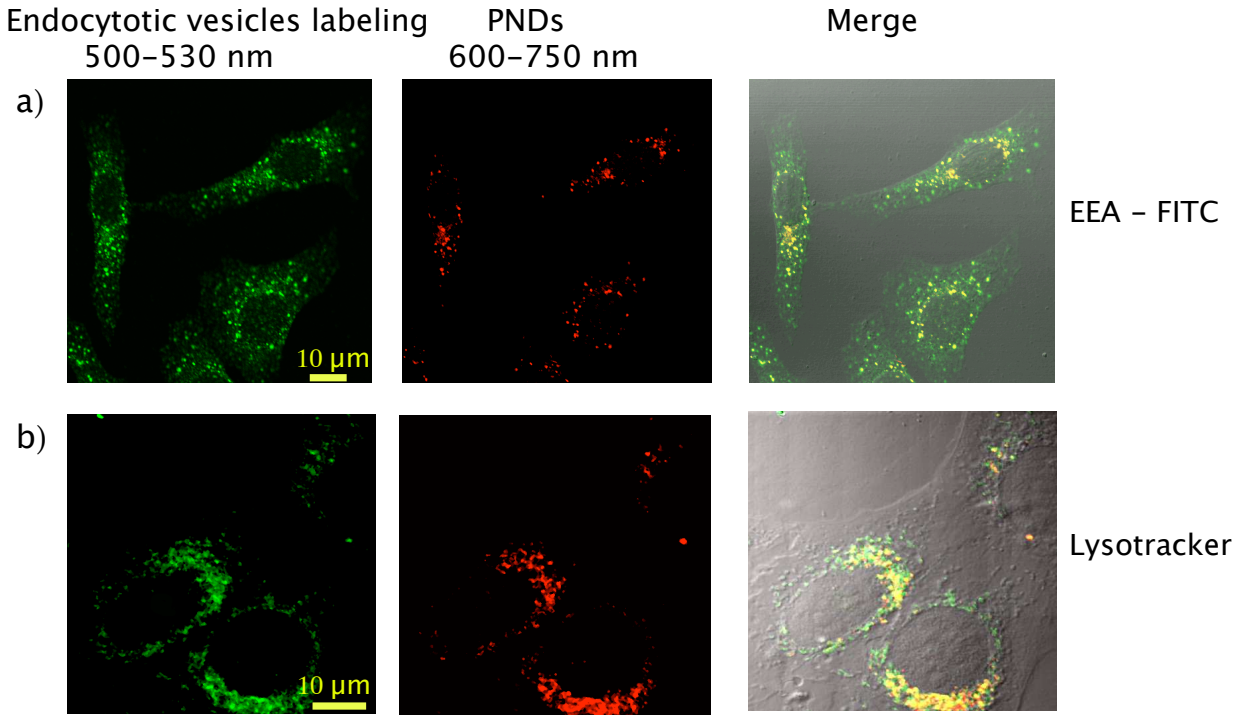

Figure 7: Localization of PNDs in HeLa cells: a) Colocalization of PNDs with early endosomes (EEA1) - FITC conjugate; b) Colocalization of PNDs with LysoTracker Green dye ; excitation wavelength 488 nm, for FITC and lysotracker dye detection range is 500-530 nm, for PNDs 600-750 nm.

In order to conclude on the partial colocalization of PNDs with endosomes and to investigate the fate of the smaller PNDs we carried out Transmission Electron Microscopy (TEM) measurements with the same type of PNDs. As it can be seen in Fig. 8a, PNDs are found in the cell cytoplasm after 2 hours of incubation.

A small portion of PNDs is not yet internalized (Fig. 8c). We check from analysis of local area Fourier transform diffractogram realized on a selected ∼10 nm nanoparticle that the observed black spots have diamond structure (inset of Fig. 8e). We observe that the PNDs trapped in vesicles are mainly in forms of aggregates (in orange color, Fig. 8b,f). Moreover we observe that a small portion of PNDs, $\sim 15\%$ of the internalized PNDs, stays free in the cytoplasm (in green, Fig. 8d).

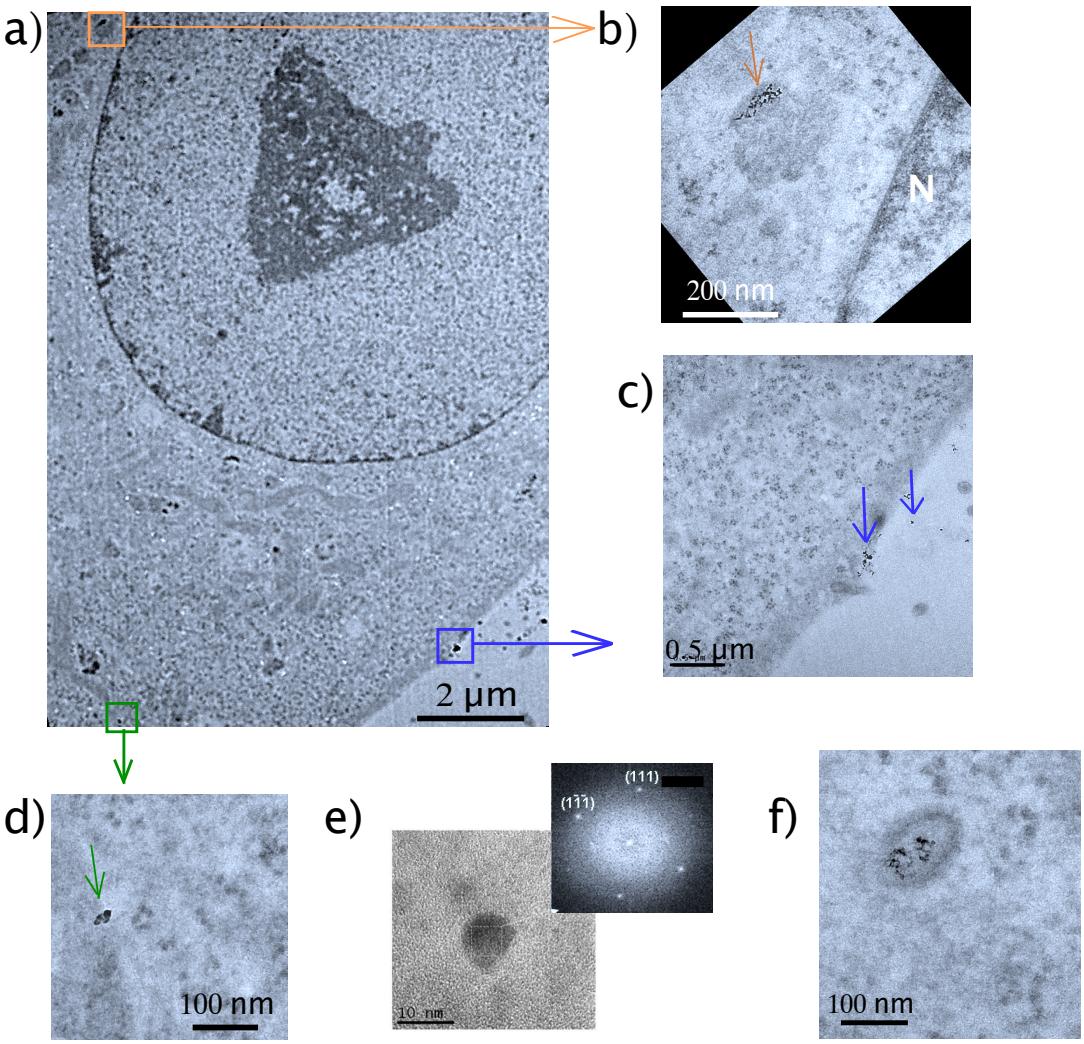

Figure 8: Transmission Electron Microscopy imaging of type 2 PNDs in HeLa cells: a) General image of a cell incubated with PNDs ; b) PNDs trapped in endocellular vesicles, N indicates the location of cell nucleus; c) PNDs not internalized or during internalization process (blue arrows) ; d) free PND in the cytoplasm; e) one 10 nm PND, inset : local area Fourier transform diffractogram; f) PNDs trapped in endocellular vesicles, image from another cell region.

PNDs - serum proteins conjugation

PNDs were incubated with cells in culture medium supplemented with 10% Fœtal Calf Serum (FCS). FCS contains various kinds of proteins with the bovine serum albumin (BSA) being the dominant one. We thus wondered whether the uptake of PNDs may be influenced by nonspecific adsorption of serum proteins onto their surface. This attachment could enhance the receptor-mediated endocytosis mechanism, as found recently for gold nanoparticle (49).

To verify this statement, we measured the ζ-potential of the PNDs - serum proteins solution, after a 2 hours incubation period, followed by extensive centrifugations and washings to eliminate the excess of proteins. The serum proteins coated PNDs exhibit a ζ-potential value of -15,6 mV (pH 7), showing a 2.5 fold decrease compared to pristine PNDs. This result is in accordance with previous studies, where BSA was used as a stabilizer for Al_2O_3 or gold nanoparticles colloidal suspensions and a similar change of the ζ-potential was observed (50, 51). The suspension remained stable for many hours after the initial mixture. After some days we observed formation of some aggregates (verified with DLS) which could be redispersed to the primary particles by sonication. On the other hand, when PNDs were added to DMEM without serum, after one day of incubation we observed a strong aggregation, most probably due to the high ionic strength of the DMEM.

To verify the presence of nonspecific adsorbed serum proteins on PNDs we performed FTIR spectroscopy measurements. The Transmission FTIR spectrum of pristine PNDs Fig. 9 shows a band near 1775 cm^{-1} which can be attributed to the C=O stretching mode of the carboxylic acid groups together with a weak band near 1630 cm^{-1} that can be assigned to the O-H bending of the same groups on the nanodiamond surface and the O-H bending due to the physically adsorbed water (more obvious at 3400 cm^{-1}) (21, 52).

When nanodiamonds were incubated with serum proteins we observed the appearance of IR bands characteristic to the serum proteins : the peak near 1640 cm^{-1} which represents the intramolecular hydrogen interaction stretching mode of the amide I band and the peak at 1538 cm^{-1} corresponding to the amide II band (53, 54).

After several washings of the particles, FTIR spectrum of the PNDs/serum-proteins conjugate still exhibits the two bands at 1640 and 1538 cm^{-1}. Moreover, the band near 1775 cm^{-1}, attributed to the stretching mode of the C=O bond at the nanodiamonds surface, is still present, but weaker. The simultaneous presence of these bands suggests an adsorption of the proteins on the diamond nanoparticles.

The decrease of the 1775 cm^{-1} band can be attributed to the diminution of the free carboxylic function at the PND surface due to their electrostatic interaction with the positively charged amino groups (-NH_3) of the proteins. An additional proof of the proteins adsorption on PNDs is the band at 2900 cm^{-1}, which can be attributed to CH_2/CH_3 groups of the alkyl chain of the proteins.

Cytotoxicity test

A necessary requirement to use PNDs as biomolecule markers is that they should present a low cytotoxicity. As cytotoxicity depends on the cellular type used and the size, shape and charge of the PNDs, we performed MTT assays for both types of nanoparticles used. Fig 10 presents the survival rate as measured with MTT assay for both proton and electron irradiated nanodiamonds. Lipofectamine, a well known nucleic acid drug vector, was used here as a comparative control. The incubation time was 24 hours. We observed that both types of PNDs do not significantly induce cell death at low doses while at high doses they appear to be less toxic than lipofectamine.

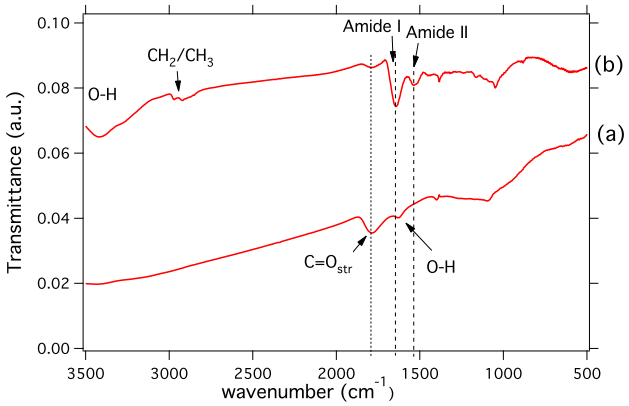

Figure 9: FTIR spectra of functionalized nanodiamonds: a) pristine PNDs ; b) PNDs - serum proteins conjugates.

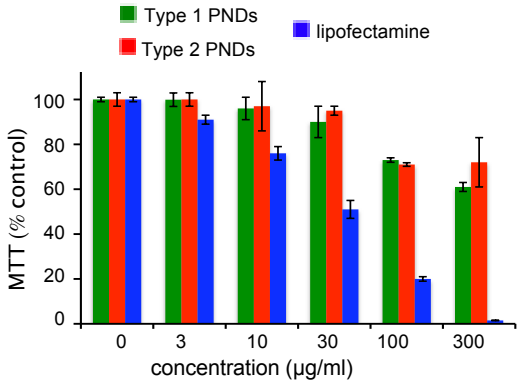

Figure 10: MTT cytotoxicity assay performed after 24 h of incubation with both nanodiamond types and lipofectamine. A similar trend of biocompatibility is observed with both type 1 and 2 of PNDs, in contrast to lipofectamine which appears to be toxic for concentrations $> 10\mu$g/ml.

Discussion

Photoluminescence properties of PDNs

In this work we compare the photoluminescence properties of a single NV center from an isolated single nanodiamond with that of a single dye molecule. We demonstrate that under ambient conditions, single NV containing nanodiamonds have a perfect photostability, while single organic molecules photobleach after a few seconds of illumination.

By fitting the acquired experimental data with the three-level model expression with an intensity dependent triplet lifetime, which corresponds well to previous calculations (33, 34), we calculate that the saturation intensity for a single molecule is 6 MW/cm^2 and the saturation fluorescence emission rate is ∼7000 kcounts/s. The value of the saturation fluorescence emission rate is relatively high, but never obtained due to photobleaching. Before photobleaching occurs, the emission rate of a single molecule is ∼70kcounts/s, a value close to the photoluminescence emission rate obtained by a single NV center (∼55 kcounts/s). The saturation intensity for a single molecule is found ∼ 3 times higher than the saturation excitation intensity required for a NV center. This result can be explained by the difference in the absorption cross section σ of the two types of emitters. The absorption cross-section was inferred in the range $\sigma_{\mathrm{cy}} \approx 4 - 6 \times 10^{-16}$ cm^2 (35) at 532 nm excitation wavelength for the cyanine molecules, while for the NV center $\sigma_{\mathrm{NV}} \approx 3 \times 10^{-17}$ cm^2 (55).

The excitation intensity at saturation (I_{sat}) is proportional to $(\sigma\tau)^{-1}$ (τ the emitter radiative lifetime), and the lifetime of cyanine is ∼6 times lower than that of the NV color center in nanodiamonds ($\tau_{\mathrm{cy}} \approx 3 - 5$ ns and $\tau_{\mathrm{NV}} \approx 15 - 25$ ns). A minimal value of $\mathrm{I}^{\mathrm{sat}}_{\mathrm{NV}}/I^{\mathrm{sat}}_{\mathrm{cy}} = 1.2$ is then expected, which is only 3.5 times higher than the one observed experimentally. This discrepancy is due to the low number of molecules and NV centers studied and the wide dispersion of the emitters radiative lifetimes which leads to non statistically significant measurements .

The possibility to increase the concentration of NV centers in nanodiamonds would enhance their natural photoluminescence, reported in (20) and allow a better detection for marking applications in biology. A way to improve the photoluminescence properties is to increase the vacancies created in the diamond matrix by high energy beam irradiation. We found here that a ten fold increase of the proton irradiation dose, from 5×10^{15} H$^+$/cm^2 to 5×10^{16} H$^+$/cm^2 leads to a three fold increase of the photoluminescence signal. It is worthy to note that such dose is the highest proton irradiation dose used so far for this type of applications.

The 5×10^{15} H$^+$/cm^2 dose produces 5×10^{16} vacancies/cm^2 while the 5×10^{16} H$^+$/cm^2 dose produces 5×10^{17} vacancies/cm^2 (55, 56). We observed a mean value of 7 NV centers in 30 nm PNDs for the highest dose. This means that 1500 vacancies have to be created to achieve the formation of a single NV center. We conclude that for the diamond type used to significantly increase the number of NV centers we do not need to create more vacancies, as a 30 nm nanodiamond, with ∼100 ppm nitrogen initial concentration, contains 480 nitrogen atoms.

A way to increase the PNDs brightness is to improve the conversion rate of non-complexed vacancies and nitrogen atoms to NV centers. The conversion percentage of 25 - 30% determined in previous studies (55, 56) is not yet achieved for nanodiamonds and gives a lot of margin for further improvement, a work that is in progress in our team.

The mean value of 7 NV centers in a 30 nm nanodiamond indicates that its photoluminescence signal is relatively high, even equivalent or higher to a commercial Quantum Dot. In a previous work we reported that a nanodiamond with 4-5 NV centers yields a photoluminescence signal equivalent to that of a Quantum Dot (14). Thus the 30 nm PNDs used in this experiment are very promising for

biological labeling applications.

Receptor Mediated Endocytosis and intracellular localization of PNDs

Previous studies have shown that PNDs may be spontaneously internalized by different cell lines using various detection techniques such as fluorescence microscopy or Raman scattering (15, 16, 20).

We show here for the first time that the internalization pathway of PNDs in cells is the endocytosis and more specifically receptor-mediated (RME), temperature and energy dependent (Fig. 5, 6).

Our results suggest that the uptake mechanism of PNDs is similar to the one observed for other nanoparticles internalized by HeLa cells, like gold nanoparticles (49) or single-walled carbon nanotubes noncovalently conjugated with DNA molecules or proteins (57).

In the case of PNDs, we attribute the RME endocytosis to the presence of the non specific adsorption of the serum proteins on the negatively charged nanoparticles surface. Analyzing the PNDs-serum proteins conjugates with FTIR spectroscopy, the bands at the amide modes region (amide I and II) demonstrate the presence of primary amines on the nanoparticles surface (Fig. 9).

Interestingly the 1775 cm^{-1} band of PNDs, attributed to C=O stretching, is drastically decreased for PNDs conjugated with serum proteins. It can be attributed to the relative diminution of the carboxylic function of the PND surface due to electrostatic interaction with the positively charged amino groups (-NH_3) of the proteins. The decrease of zeta potential confirms this statement. This diminution could be also due to nanoparticle aggregation, but at least after 2 hours of incubation we checked (with DLS) that PNDs were still not aggregated. This diminution of the zeta potential can also explain the internalization of the PNDs. With overall initial highly negative charged surface, the electrostatic repulsion between negatively charged membranes and the particles would prevent them from entering efficiently in cells. The adsorption of the proteins on the nanodiamonds surface changes the surface charge and can facilitate internalization. Serum contains a diverse set of proteins, like BSA, transferrin, α- and β- globulin, etc. The dominant protein however is the BSA. BSA is frequently used for nanoparticles functionalization and intracellular trafficking (58, 59, 60). Very recent studies have also used the BSA coating of nanodiamonds to obtain stable suspensions in cell culture mediums (61), which is in accordance to our observations.

The above results offer the foundation for future investigations of the internalization diamond nanoparticles attached to proteins or biomolecules. Moreover, we demonstrate the colocalization of PNDs with endosomes or lysosomes, but the results also suggest that a low proportion of the nanoparticles is not colocalized with vesicular compartments and may reside in the cell cytoplasm. By TEM observations we clarify the precise localization of PNDs in cells and prove that nanodiamond-aggregates are trapped in endocellular vesicles, which is a result similar to the one obtained for gold nanoparticles studies (49, 62). Interestingly, a portion of PNDs, mainly the smaller ones ($\sim$10-15 nm) is not trapped in vesicles and rests free in the cytoplasm. Neugart et al. (12) had also indications that a small portion of PNDs diffuses freely in cells by calculating the diffusion coefficient. Whether this proportion of nanodiamonds escaped from endosomes or entered directly the cells without been trapped in them is a question that needs to be answered; we are carrying out further investigations.

Finally, as toxicity depends strongly on the nanoparticles size and shape (63) it is essential to test the biocompatibility for each type of nanodiamonds used. We show here that both PNDs type used here are not toxic in vitro after 24h. However the understanding of possible long-term adverse effects of internalized nanodiamonds on cells will require long term toxicology experiments on animal models; a remaining task for future investigations.

Conclusion

We showed that contrary to dye molecules, the emission of single NV centers in single nanodiamonds is perfectly stable in time and studied the corresponding photoluminescence behaviors. In order to improve the nanodiamonds photoluminescence yield, we tried 2 different proton irradiation doses and gained a factor of three regarding photoluminescence intensity. After calculations we conclude that there is still plenty of room to improve the conversion of the available vacancies and nitrogen atoms in the diamond matrix to NV color centers.

Additionally, we demonstrated that the internalization of PNDs in HeLa cells happens through receptor-mediated endocytosis. Serum proteins are adsorbed on the nanoparticles surface and influence their uptake. Results show that most of the nanodiamonds are localized in intracellular endocytotic vesicles in perinuclear regions, except a small portion and in particular the smallest particles that remain free in the cytoplasm, indicating that this material may be a good candidate long-term intracellular tracking of biomolecules.

Establishment of the entry mechanisms is of fundamental importance and will facilitate future developments of nanodiamonds as drug-delivery vehicles.

Acknowledgements

We are grateful to Jean-François Roch for fruitful discussions. We also thank Géraldine Dantelle for the measurements of the zeta potential, Anne Tarrade for the preparation of the samples for TEM imaging, Jacques Botsoa for the SRIM calculations and Thierry Sauvage for the proton irradiations. This work was supported by the European Commission through the project "Nano4Drugs" (contract LSHB-2005-CT-019102), by Agence Nationale de la Recherche through the project "NaDia" (contract ANR-2007-PNANO-045) and by "Ile de France" Region *C'Nano* grant under the project "Biodiam".

References

[1] P. Alivisatos. The use of nanocrystals in biological detection. *Nat. Biotec.*, 22:47–52, 2004.

[2] I.L. Medintz, H.T. Uyeda, E.R. Goldman, and H. Mattoussi. Quantum dot bioconjugates for imaging, labelling and sensing. *Nature Materials*, 4:435, 2005.

[3] S.L. Reck-Peterson, A. Yildiz, A.P. Carter, A. Gennerich, N. Zhang, and R.D. Vale. Single-molecule analysis of dynein processivity and stepping behavior. *Cell*, 126:335–348, 2006.

[4] D. Lasne, G. Blab, S. Berciaud, M. Heine, L. Groc, D. Choquet, L. Cognet, and B. Lounis. Single nanoparticle photothermal tracking (snapt) of 5-nm gold beads in live cells. *Biophys. J.*, 91:4598 – 4604, 2006.

[5] V. Zharov, K. Mercer, E. Galitovskaya, and M. Smeltzer. Photothermal nanotherapeutics and nanodiagnostics for selective killing of bacteria targeted with gold nanoparticles. *Biophys. J.*, 90:619 – 627, 2006.

[6] J.H. Warner, A. Hoshino, K. Yamamoto, and R.D. Tilley. Water-soluble photolumines- cent silicon quantum dots. *Angew. Chem. Int. Ed.*, 44:4550 – 4554, 2005.

[7] U. Resch-Genger, M. Grabolle, S. Cavaliere-Jaricot, R. Nitschke, and T. Nann. Quantum dots versus organic dyes as fluorescent labels. *Nat. Meth.*, 9:763–775, 2008.

[8] X. Michalet, F. Pinaud, L. Bentolila, J. Tsay, S. Doose, J.J. Li, G. Sundaresan, A.M. Wu, S. Gambhir, and S. Weiss. Quantum dots for live cells, in vivo imaging, and diagnostics. *Science*, 307:538–544, 2005.

[9] C. Kirchner, T. Liedl, S. Kudera, T. Pellegrino, A. Javier, H. Gaub, S. Stoelze, N. Fertig, and W.J. Parak. Cytotoxicity of colloidal cdse and cdse/zns nanoparticles. *Nano Lett.*, 5:331, 2005.

[10] M. Nirmal, B. Dabbousi, M.G. Bawendi, J.J. Macklin, J.K. Trautman, T.D. Harris, and L.E. Brus. Fluorescence intermittency in single cadmium selenide nanocrystal. *Nature*, 383:802–804, 1996.

[11] A. Gruber, A. Dräbenstedt, C. Tietz, L. Fleury, J. Wrachtrup, and C. Von Borczyskowsky. Scanning confocal optical microscopy and magnetic resonance on single defect centers. *Science*, 276:2012, 1997.

[12] F. Neugart, A. Zappe, F. Jelezko, C. Tietz, J.-P. Boudou, A. Krueger, and J. Wrachtrup. Dynamics of diamond nanoparticles in solution and cells. *Nano Lett.*, 7:3588 –3591, 2007.

[13] Y.-R. Chang, H.-Y. Lee, K. Chen, C.-C. Chang, D.-S. Tsai, C.-C. Fu, T.-S. Lim, Y.-K. Tzeng, C.-Y. Fanf, C.-C. Han, H.-C. Chang, and W. Fann. Mass production and dynamic imaging of fluorescent nanodiamonds. *Nature Biotechnology*, 3:284–288, 2008.

[14] O. Faklaris, D. Garrot, V. Joshi, J.P. Boudou, T. Sauvage, P.A. Curmi, and F. Treussart. Comparison of the photoluminescence properties of semiconductor quantum dots and non-blinking diamond nanoparticles. observation of the diffusion of diamond nanoparticles in living cells. *arXiv:0904.2648 and J. Europ. Opt. Soc. Rap. Public.*, 4, 2009.

[15] C.-C. Fu, H.-Y. Lee, K. Chen, T.-S. Lim, H.-Y. Wu, P.-K. Lin, P.-K. Wei, P.-H. Tsao, H.-C. Chang, and W. Fann. Characterization and applications of single fluorescent nanodiamonds as cellular biomarkers. *Proc. Nat. Acad. Sc.*, 104:727, 2007.

[16] O. Faklaris, D. Garrot, V. Joshi, F. Druon, J.P. Boudou, T. Sauvage, P. Georges, P.A. Curmi, and F. Treussart. Detection of single photoluminescent diamond nanoparticles in cells and study of their internalization pathway. *Small*, 4:2236–2239, 2008.

[17] A. M. Schrand, H. Huang, C. Carlson, J. Schlager, E. Osawa, S.M. Hussain, and L. Dai. Are diamond nanoparticles cytotoxic? *J. Phys. Chem. B*, 111(1):2–7, JAN 11 2007.

[18] H. Huang, E. Pierstorff, E. Osawa, and D. Ho. Active nanodiamond hydrogels for chemotherapeutic delivery. *Nano Lett.*, 7(11):3305–3314, NOV 2007.

[19] A. Krüger. Diamond nanoparticles for biological applications. *J. Chem. Eur.*, 14:1382, 2008.

[20] J.-I. Chao, E. Perevedentseva, P.-H. Chung, K.-K. Liu, C.-Y. Cheng, C.-C. Chang, and C.-L. Cheng. Nanometer-sized diamond particle as a probe for biolabeling. *Biophys. J.*, 93:2199, 2007.

[21] S. Vial, C. Mansuy, S. Sagan, T. Irinopoulou, F. Burlina, J.P. Boudou, G. Chassaing, and S. Lavielle. Peptide-grafted nanodiamonds: preparation, cytotoxicity and uptake in cells. *ChemBioChem*, 9:2113–2119, 2008.

[22] J.P. Boudou, P.A. Curmi, F. Jelezko, J. Wrachtrup, P. Aubert, M. Sennour, G. Balasubramanian, R. Reuter, A. Thorel, and E. Gaffet. High yield fabrication of fluorescent nanodiamonds. *Nanotechnology*, 20(235602), 2009.

[23] Y. Sonnefraud, O. Faklaris A. Cuche, J.-P. Boudou, T. Sauvage, J.-F. Roch, F. Treussart, and S. Huant. Diamond nanocrystals hosting single nv color centers sorted by photon-correlation near-field microscopy. *Opt. Lett.*, 33:611, 2008.

[24] F. Treussart, V. Jacques, E Wu, T. Gacoin, P. Grangier, and J.-F. Roch. Photoluminescence of single colour defects in 50 nm diamond nanocrystals. *Physica B*, 376:926–929, 2006.

[25] F.T. Mu, J. Callaghan, O. Steele-Mortimer, H. Stenmark, R. Parton, P. Campbell, J. Mccluskey, Y. Jing-Ping, E. Tock, and T. Ban-Hock. Eea1, an early endosome- associated protein. eea1 is a conserved alpha-helical peripheral membrane protein flanked by cysteine "fingers" and contains a calmodulin-binding iq motif. *J Biol Chem.*, 270:13503–13511, 1995.

[26] J. Carmichael, W.D. DeGraff, A.F. Gazdar, J.B. Minna, and J. Mitchell. Evaluation of a tetrazolium-based semiautomated colorimetric assay: Assessment of chemosensitivity testing. *Cancer Res.*, 47:936–942, 1987.

[27] S. Weiss. Fluorescence spectroscopy of single biomolecules. *Science*, 283:1676, 1999.

[28] W. E. Moerner. New directions in single-molecule imaging and analysis. *Proc. Natl. Acad. Sci. USA*, 104:12596–12602, 2007.

[29] F. Treussart, R. Alléaume, V. Le Floc'h, L.T. Xiao, J.-M. Courty, and J.-F. Roch. Direct measurement of the photon statistics of a triggered single photon source. *Phys. Rev. Lett.*, 89:093601, 2002.

[30] F. Hashimoto, S. Tsukahara, and H. Watarai. Lateral diffusion dynamics for single molecules of fluorescent cyanine dye at the free and surfactant-modified dodecane- water interface. *Langmuir*, 19:4197–4204, 2003.

[31] S.C. Blanchard, H.D. Kim, R.L. Gonzalez, J.D. Puglisi, and S. Chu. trna dynamics on the ribosome during translation. *Proc. Natl. Acad. Sci. USA*, 101:12893–12898, 2004.

[32] L.S. Churchman, Z. Okten, R.S. Rock, J.F. Dawson, and J.A. Spudich. Single molecule high-resolution colocalization of cy3 and cy5 attached to macromolecules measures intramolecular distances through time. *Proc. Natl. Acad. Sci. USA*, 102:1419–1423, 2005.

[33] F. Treussart, A. Clouqueur, C. Grossman, and J.-F. Roch. Photon antibunching in the fluorescence of a single dye molecule embedded in a thin polymer film. *Opt. Lett.*, 26:1504, 2001.

[34] T. Basche, W.E. Moerner, M. Orrit, and U.P. Wild. *Single-Molecule Optical Detection, Imaging and Spectroscopy.* VCH, Weinheim, Germany, 1st edition, 1997.

[35] H. Gruber, C. Hahn, G. Kada, C. Riener, G. Harms, W. Ahrer, T. Dax, and H.G. Knaus. Anomalous fluorescence enhancement of cy3 and cy3.5 versus anomalous fluorescence loss of cy5 and cy7 upon covalent linking to igg and noncovalent binding to avidin. *Bioconj. Chem.*, 5:696–704, 2000.

[36] A. Beveratos, R. Brouri, T. Gacoin, J.-Ph. Poizat, and Ph. Grangier. Nonclassical radiation from diamond nanocrystals. *Phys. Rev. A*, 64:061802, 2001.

[37] L. Allers, A.T. Collins, and J. Hiscock. The annealing of interstitial-related optical centres in type ii natural and cvd diamond. *Diamond Relat. Mater.*, 7:228–232, 1998.

[38] N.B. Iakoubovskii and G.J. Adrianenssens. Trapping of vacancies by defects in diamond. *J. Phys. C*, 13:6015–6018, 2001.

[39] M. Marsh and H.T. McMahon. Cell biology - the structural era of endocytosis. *Science*, 285:215, 1999.

[40] E.D. Gundelfinger, M.M. Kessels, and B. Qualmann. Temporal and spatial coordination of exocytosis and endocytosis. *Nature Rev. Mol. Cell Biol.*, 2:127–139, 2003.

[41] S. Murkherjee, R.N. Ghosh, and F.R. Maxfield. Endocytosis. *Physiol. Rev.*, 77:759–803, 1997.

[42] S.L. Schmid and L.L. Carter. Atp is required for receptor-mediated endocytosis in intact cells. *J. Cell Biol.*, 111:2307–2318, 1990.

[43] A. Jones, M. Gumbleton, and R. Duncan. Understanding endocytic pathways and in- tracellular trafficking: a prerequisite for effective design of advanced drug delivery systems. *Adv. Drug Deliv. Rev.*, 55:1353 1357, 2003.

[44] R. Steinman, I. Mellman, W. Muller, and Z. Cohn. Endocytosis and the recycling of plasma membrane. *J. Cell Biol.*, 96:1–27, 1983.

[45] S.A. Mousavi, L. Malerod, T. Berg, and R. Kjeken. Clathrin-dependent endocytosis. *Biochem. J*, 377:1–16, 2004.

[46] L. Pelkmans, T. Brli, M. Zerial, and A. Helenius. Caveolin-stabilized membrane domains as multifunctional transport and sorting devices in endocytic membrane traffic. *Cell*, 118:767–780, 2004.

[47] J. Heuser and R.G. Anderson. Hypertonic media inhibit receptor-mediated endocytosis by blocking clathrin-coated pit formation. *J. Cell Biol.*, 108:389–400, 1989.

[48] M. Qaddoumi, H. Gukasyan, J. Davda, V. Labhasetwar, K.J. Kim, and V. Lee. Clathrin and caveolin-1 expression in primary pigmented rabbit conjunctival epithelial cells: Role in plga nanoparticle endocytosis. *Molec. Vis.*, 9:559–568, 2003.

[49] B.D. Chithrani, A.A. Ghazani, and W.-C. Chan. Determining the size and shape dependence of gold nanoparticle uptake into mammalian cells. *Nano Lett*, 6:662– 668, 2006.

[50] K. Rezwan, L.P. Meier, M. Rezwan, J. Voros, M. Textor, and L.J. Gauckler. Bovine serum albumin adsorption onto colloidal alo particles: A new model based on zeta potential and uv-vis measurements. *Langmuir*, 20:10055–10061, 2004.

[51] S. H. Brewer, W.R. Glomm, M.C. Johnson, M.K. Knag, and S. Franzen. Probing bsa binding to citrate-coated gold nanoparticles and surfaces. *Langmuir*, 21:9303–9307, 2005.

[52] P.-H. Chung, E. Perevedentseva, J.-S. Tu, C.-C. Chang, and C.-L. Cheng. Spectroscopic study of bio-functionalized nanodiamonds. *Diam. Relat. Mater.*, 15:622, 2005.

[53] V. Militello, C. Casarino, A. Emanuele, A. Giostra, F. Pullara, and M. Leone. Aggregation kinetics of bovine serum albumin studied by ftir spectroscopy and light scattering. *Bioph. Chem.*, 107:175187, 2004.

[54] K. Murayama and M. Tomida. Heat-induced secondary structure and conformation change of bovine serum albumin investigated by fourier transform infrared spectroscopy. *Biochem.*, 43:11526–11532, 2004.

[55] T.-S. Wee, Y.-K. Tzeng, C.-C. Han, H.-C. Chang, W. Fann, J.-H. Hsu, K.-M. Chen, and Y.-C. Yu. Two-photon excited fluorescence of nitrogen-vacancy centers in proton-irradiated type ib diamond. *J. Phys. Chem. A*, 111:9379–9386, 2007.

[56] S.C. Lawson, D. Fisher, D. Hunt, and M. Newton. On the existence of positively charged single- substitutional nitrogen in diamond. *J. Phys. Condens. Matter*, 10:6171 6180, 1998.

[57] N.W.S. Kam, Z. Liu, and H. Dai. Carbon nanotubes as intracellular transporters for proteins and dna : An investigation of the uptake mechanism and pathway. *Angew. Chem. Int. Ed.*, 45:577–581, 2006.

[58] A. Tkachenko, H. Xie, D. Coleman, W. Glomm, J. Ryan, M.F. Anderson, S. Franzen, and D. Feldheim. Multifunctional gold nanoparticle-peptide complexes for nuclear targeting. *J. Am. Chem. Soc.*, 16:4700–4701, 2003.

[59] A. Derfus, W.-C. Chan, and S. Bhatia. Intracellular delivery of quantum dots for live cell labelling and organelle tracking. *Adv.Matt.*, 16(12), 2004.

[60] C.-H. Yu, A. Al-Saadi, S.-J. Shih, L. Qiu, K.-Y. Tam, and S.-C Tsang. Immobilization of bsa on silica-coated magnetic iron oxide nanoparticle. *J. Phys. Chem. C*, 113:537–543, 2009.

[61] Y. Yuan, Y. Chen, J.-H. Liu, H. Wang, and Y. Liu. Biodistribution and fate of nanodiamonds in vivo. *Diam. Rel. Mat.*, 18:95100, 2009.

[62] P. Nativo, I.A. Prior, and M. Brust. Uptake and intracellular fate of surface-modied gold nanoparticles. *ACS Nano*, 2:1639 1644, 2008.

[63] N. Lewinski, V. Colvin, and R. Drezek. Cytotoxicity of nanoparticles. *Small*, 4:26 49, 2008.